TU Delft

Delft University of Technology

The effect of slag chemistry on the reactivity of synthetic and commercial slags

Zhang, Yu; Zhang, Shizhe; Chen, Yu; Çopuroğlu, Oğuzhan

DOI
10.1016/j.conbuildmat.2022.127493

Publication date
2022

Document Version
Final published version

Published in
Construction and Building Materials

Citation (APA)
Zhang, Y., Zhang, S., Chen, Y., & Çopuroğlu, O. (2022). The effect of slag chemistry on the reactivity of synthetic and commercial slags. *Construction and Building Materials*, *335*, 1-12. Article 127493. https://doi.org/10.1016/j.conbuildmat.2022.127493

Important note
To cite this publication, please use the final published version (if applicable).
Please check the document version above.

Copyright
Other than for strictly personal use, it is not permitted to download, forward or distribute the text or part of it, without the consent of the author(s) and/or copyright holder(s), unless the work is under an open content license such as Creative Commons.

Takedown policy
Please contact us and provide details if you believe this document breaches copyrights.
We will remove access to the work immediately and investigate your claim.

This work is downloaded from Delft University of Technology.
For technical reasons the number of authors shown on this cover page is limited to a maximum of 10.

Construction and Building Materials 335 (2022) 127493

Contents lists available at ScienceDirect

Construction and Building Materials

journal homepage: www.elsevier.com/locate/conbuildmat

The effect of slag chemistry on the reactivity of synthetic and commercial slags

Yu Zhang *, Shizhe Zhang, Yu Chen, Oğuzhan Çopuroğlu

Microlab, Section of Materials and Environment, Faculty of Civil Engineering and Geosciences, Delft University of Technology, Delft, the Netherlands

ARTICLE INFO

Keywords:
Synthetic and commercial slags
Reactivity
Chemical composition
Graphical method
Sulfur species

ABSTRACT

In this paper, both synthetic slag and commercial slag covering the common composition range were employed to estimate the correlation between slag chemistry and reactivity through hydraulicity and dissolution tests. It was found that slag reactivity was favorably affected by increasing Al_2O_3 and MgO contents, while the adverse effect of decreasing CaO/SiO_2 ratio could be compensated by higher amounts of Al_2O_3 and/or MgO. When calorimetric measurement was used to assess the reactivity of slag, the effect of sulfur species incorporated in commercial slag should be taken into consideration as a small quantity of it could lead to a major difference of cumulative heat release due to the formation of ettringite. Moreover, a novel graphical method was proposed to estimate the reactivity of slag considering its chemical composition from a new perspective, i.e. a cartesian coordinate system based on (CaO/SiO_2)–$(MgO + Al_2O_3)$.

1. Introduction

In order to contribute the efforts towards reaching carbon neutrality target worldwide by 2050, cement and concrete industry has been exploring possibilities to use various supplementary cementitious materials (SCMs) in binders. These sustainable SCMs are considered favorable for reducing raw material depletion and the use of thermal and electric energy, therefore leading to significantly lower CO_2 emissions [1–3].

Blast furnace slag (henceforth slag), a widely used SCM in Europe and north American countries, is a by-product of iron/steel manufacturing. Compared with ordinary portland cement, the amount of C–S–H formed upon slag cement hydration is higher whereas its Ca/Si ratio is lower due to higher silica and lower lime content in a typical slag composition. Portlandite, C–S(A)–H gel phase, ettringite, AFm phases and a hydrotalcite-like phase are the common products identified in a typical hydrated slag cement system [4–6].

Slag consists of a three dimensional interconnected network structure and is mainly composed of – more than 90% on average – glassy phase, which is responsible for its latent hydraulic property. The chemical composition of slag varies depending on iron ore, fluxing stone and impurity of the coke fed into the blast furnace. When SiO_2 and Al_2O_3 are combined with CaO and MgO, the molten slag floats on top of the iron liquid at the bottom of blast furnace due to the difference of their densities. Therefore, slag is rich in calcium oxide and silica (major constituents), with significant amount of alumina and magnesium oxide (minor constituents), and can be expressed as a $CaO–SiO_2–Al_2O_3–MgO$ system. Shimoda et al. [7] concluded that the polymerization structure of Si in slag was close to chain-like linkage, namely $Q^2(1Al)$ and $Q^2(2Al)$. Moreover, there is a consensus existing that in case of the presence of large amount of Al_2O_3 ($Al_2O_3 \geq 0.5\ SiO_2$ in molar ratio), except for the four-fold coordinated Al considered as network former existing only in-between SiO_4 tetrahedra in the form of Si–O–Al–O–Si (Loewenstein's rule of aluminum avoidance [8]), some aluminum are also in five- and six-fold coordination states and regarded as network modifier as it is an amphoteric oxide [9,10]. On the other hand, the field strength, z/r^2 ratio (z and r, are the charge and radius of cation, respectively), represents the strength of bond between a non-bridging oxygen and a cation, playing a key role in modification of the glass structure [11,12]. It is well concluded that a cation with larger z/r^2 (i.e. Mg^{2+}) tends to generate lower degree of polymerization. The order of field strength among cations commonly seen in slag follows $K^+ < Na^+ < Ca^{2+} < Mg^{2+}$ [13]. In the network structure of slag, Mg^{2+} with smaller radius tends to act as network modifier while Ca^{2+} performs charge compensation. Results from [14,15] also concluded that MgO in slag has relatively small ion radii which may present stronger capacity to break the linkage of network structure.

In order to assess the quality/reactivity of blast furnace slag (the rate

* Corresponding author.
E-mail address: Y.Zhang-28@tudelft.nl (Y. Zhang).

https://doi.org/10.1016/j.conbuildmat.2022.127493
Received 28 January 2022; Received in revised form 30 March 2022; Accepted 10 April 2022
Available online 18 April 2022
0950-0618/© 2022 The Author(s). Published by Elsevier Ltd. This is an open access article under the CC BY license (http://creativecommons.org/licenses/by/4.0/).

of slag reaction with alikalis released by cement), much efforts have been made to observe a relationship that could be used to predict slag reactivity from its chemical composition [16,17]. Several different hydraulic moduli (or basicity) were reviewed in the literature, e.g. [18]. However, none of them gives a satisfactory result for estimating various slag used in cement [17,19]. The effect of the four main metal oxides on the reactivity of slag was individually investigated since early 1900s. It was found that CaO and MgO in slag basically had a positive effect on reactivity, whereas SiO_2 had a negative influence [20–23]. A deficiency in CaO could be compensated by MgO, as stated in EN 15167-1. Keeping the basicity index (CaO/SiO_2) constant, increasing the amount of Al_2O_3 in slag promotes the early age compressive strength development [24,25]. The authors in [26] connected the higher compressive strength to the higher ettringite content produced, with a higher degree of space filling. However, it was also found that increasing Al_2O_3 content of slag slowed down the early hydration and a lower compressive strength during the first days was observed in alkali-activated slag system [27].

In the recent years, several researchers studied synthetic $CaO–SiO_2–Al_2O_3$ based glasses with controlled chemical composition in the laboratory conditions [28–31] to simulate the performance of SCMs in blended commercial cements. This approach was particularly preferred in order to eliminate potential interferences from other internal or external sources. These studies showed that chemical composition played a key role on the slag network structure, which affects the surface free energy, hence its reactivity. It is generally recognized that the reactivity increases with increasing depolymerization of the silicate structure. The works in [32] extended the glass further into $CaO–SiO_2–Al_2O_3–MgO$ system and confirmed that when substituted with Ca, Mg only slightly affected the aluminosilicate network structure, although an increased distortion of network structure was observed. With the increasing of MgO + CaO content, the network depolymerization and thus the glass reactivity increased correspondingly, on which the Mg substitution had only a minor impact.

In this paper, nine synthetic slags based on $CaO–SiO_2–Al_2O_3–MgO$ system and one commercial slag were considered. The idea behind the design of synthetic slags was to cover the entire range of composition typically encountered in commercial slags. These slags were characterized by XRD, ESEM, as well as FTIR. Meanwhile, in order to study reactivity, two methods were used in the study. The first one was hydraulicity/R3 test on a model blended system composed of slag, calcium hydroxide, limestone and potassium-hydroxide and -sulfate solutions. The aim of this blended system is to simulate the environment occurring in a hydrating slag cement [33–36]. The other test was the dissolution test of slag in strong NaOH solution. In principle, the hydration process could be recognized as a couple of reactions involving dissolution of raw material and precipitation of hydrates. Therefore, a more underlying insight into the dissolution process of slag in alkaline solution is essential to understand the pozzolanic reaction between slag and calcium hydroxide [37–39]. Additionally, we attempted to estimate the reactivity of slag using a novel graphical method based on a cartesian coordinate system of $(CaO/SiO_2)–(MgO + Al_2O_3)$ in weight percentage.

This study provides a new insight on the influence of chemical composition on the reactivity of synthetic slag, using a novel graphical approach. The suggested methodology could contribute to the evaluation of reactivity test and could lead to formulating improved blast furnace slag composition for better durability performance.

2. Material and methodology

2.1. Synthesis and characterization of slag

Nine synthetic slags (M0, M8, M16; A3, A3-1, A12, A18; CS1, CS2), one commercially available slag (S) (Ecocem Benelux B.V.), and Quartz powder (Qz) were used in the study. The synthetic slag was prepared by mixing commercial slag S with AR (analytical reagent) CaO, MgO, SiO_2, Al_2O_3 according to different compositional design targets. The commercial slag S and analytical reagents added to control the exact composition in each run were mixed into a homogeneous blend by combining the materials with pure ethyl alcohol, grinding the mixture in a ball milling machine at a low speed for 2 h and drying them at 100 °C for 24 h. The dried material was then ground to finer than 200 μm using a mortar and pestle for improved homogeneity. Then, it was melted in an Al_2O_3 crucible at 1550 °C in the oven (High temperature furmace, Carbolite) for 3 h (heated from room temperature to 1550 °C at 10 °C/min and maintained at 1550 °C for 3 h). The molten liquid was water quenched to obtain glassy slag, rinsed with isopropanol and dried at 100 °C for 24 h, subsequently. Finally, it was crushed and ground down to the required particle size distribution in a ball mill (Retsch PM 100).

The chemical composition of the materials are presented in Table 1. Their particle size distributions were measured by laser diffraction and are shown in Fig. 1. It is obvious that they have a similar d50. In M series, CaO/SiO_2 ratio was kept at around 1 and the amount of Al_2O_3 fluctuated at around 14%, while MgO content were determined from 0.33% to 16.07%. Similarly, for A3, A12 and A18 in A series, CaO/SiO_2 ratio was also maintained at around 1.0 and the amount of MgO was stabilized at about 10%, while Al_2O_3 content varied from 3.69% to 18.19%. As for synthetic slag A3-1 in A series, it contained almost the same amount of MgO and Al_2O_3 compared with the slag A3 while the amount of CaO was ~10% less than that of SiO_2. The purpose of CS series was to investigate the effect of CaO/SiO_2 ratio on the reactivity of slag, and the MgO and Al_2O_3 contents levelled-off at approximately 10% and 15%, respectively. Especially for CS2, the $(CaO + MgO)/SiO_2$ ratio of which was less than 1, which does not conform the European Standard EN 15167-1. Commercial slag S was used as a reference and had a similar chemical composition with the synthetic slag M8.

2.2. Characterization of the structure of synthetic slag

X-ray diffraction (XRD) measurement was employed to determine possible crystal phase formations. It was performed on a Philips PW 1830/40 Powder diffractometer employing the Cu K-alpha radiation (employing Bragg-Brentano reflection geometry). The machine was operated with an acceleration voltage of 40 kV and an X-ray beam current of 40 mA. Analysis was performed with a step size of 0.03°, for a 2θ range from 5° to 60°.

Another part of slag powders were further coated with carbon to examine their morphology using FEI QUANTA FEG 650 ESEM with an accelerating voltage of 15 kV and at a working distance of 10 mm in secondary electron (SE) detection mode. Morphology between the synthetic slags and the commercial slag was compared based on SE micrographs.

Fourier transform infrared spectroscopy was performed using Spectrum TM 100 Optical ATR-FTIR spectrometer over the wavelength range from 600 to 1600 cm^{-1} to identify the chemical bonding environment of Si structural units. A single-beam configuration was used, and each sample was scanned 20 times with a fixed instrument resolution of 4 cm^{-1}.

2.3. Characterization of slag reactivity

2.3.1. Hydraulicity test

The composition of the model system used here is shown in Table 2. Details of the method can be found elsewhere [33-36]. Calcium hydroxide was used to trigger puzzolanic activity. A very small quantity of limestone ($CaCO_3$) was added to facilitate reactions with the dissolved aluminum from slag. Potassium hydroxide and potassium sulfate were combined in certain proportion and dissolved in reagent water to obtain dissolved ions such as SO_4^{2-} and OH^- to mimic the pore solution of slag cement.

40 °C calorimetry was performed over 7 days. Within 5 min after mixing, paste was casted into an air-tight specimen container and

Table 1
Chemical compositions (wt.%) determined by XRF and physical properties of these ten slags.

	M0	M8	M16	A3	A3-1	A12	A18	CS1	CS2	S
CaO	43.16	37.04	34.09	42.07	38.39	37.32	36.87	**32.98**	**28.05**	37.40
SiO_2	42.99	37.79	32.99	43.30	48.41	39.11	34.43	**38.67**	**42.84**	37.82
Al_2O_3	13.30	14.51	15.05	**3.69**	**2.39**	**12.32**	**18.19**	14.51	17.12	13.58
MgO	**0.33**	**8.83**	**16.07**	10.83	10.58	9.43	7.98	11.22	9.67	8.11
FeO/Fe_2O_3	0.07	0.28	0.34	0.07	0.09	0.30	0.40	0.36	0.35	0.36
TiO_2	–	0.70	0.73	–	–	0.70	0.84	1.02	0.89	1.22
MnO/Mn_2O_3	–	0.17	0.16	–	–	0.15	0.27	0.22	0.19	0.3
Na_2O	–	0.24	0.22	–	0.07	0.24	0.37	0.36	0.31	–
K_2O	–	0.25	0.21	–	–	0.21	0.41	0.36	0.32	0.28
SO_3	0.01	0.01	0.01	0.01	0.01	0.03	0.03	0.05	0.08	0.93
Residual	0.14	0.18	0.13	0.03	0.06	0.19	0.21	0.25	0.08	–
CaO/SiO_2	1.00	0.98	1.03	0.97	0.79	0.95	1.07	0.85	0.65	0.99
$(CaO + MgO)/SiO_2$ [a]	1.01	1.21	1.52	1.22	1.01	1.20	1.30	1.14	0.88	1.20
NBO/T [b]	1.33	1.67	2.10	2.48	2.17	1.80	1.53	1.64	1.15	1.73
Physical properties										
d_{50} (μm) [c]	24.35	22.73	22.29	19.67	20.69	20.35	20.85	20.40	20.11	20.94
SSA (m^2/g) [d]	0.77	0.90	0.96	1.09	0.91	0.92	0.90	0.93	1.08	0.94

a. The European Standard EN 15167-1 recommends that the ratio should be greater than 1.
b. The degree of depolymerization of slag network structure can be represented by NBO/T, the number of non-bridging oxygen (NBO) per tetrahedral network-forming element (T), following the equation proposed in [40].
c. The particle size distribution (PSD) of these slags was measured by EyeTech, Ankersmid. The d_{50} of quartz is 24.21 μm.
d. The specific surface area (SSA) of these slags was measured by nitrogen adsorption with 11-point BET method (Micrometritics, Gemini VII 2390p). The slag powders were dried at 105 °C and degassed before the experiments. The analytical error is in limit of ±2%. Comparatively, a low specific surface area was obtained for slag M0, which was partially due to its relatively coarser particle size distribution as reflected by the d_{50}.

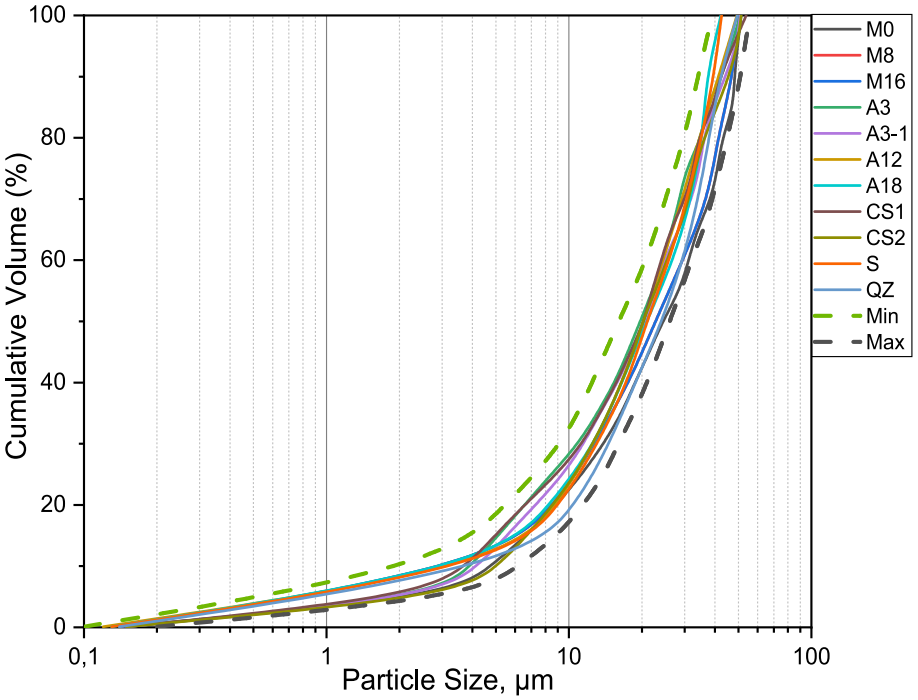

Fig. 1. Particle size distribution of slag and quartz.

Table 2
Components (gram) of the blended system.

	Syn. Slag	Portlandite	Limestone	Potassium solution [a]
Blended system	10.0	30.0	5.0	54

[a] Potassium solution was prepared by dissolving 4.0 g of potassium hydroxide and 20.0 g of potassium sulfate in 1.0 L of reagent water (pH ≈ 12.85) conditioned at 20 ± 3 °C.

transferred into the equipment. In addition, paste samples were also casted in 20 mL plastic bottle and cured under 40 °C for 7 days for further investigation. Elevated temperature (40 °C) was employed to accelerate the rate of reaction between slag and calcium hydroxide. Also, 7 days was considered to be sufficient enough to determine the level of reactivity and the variability of test results was low [33,35,36].

Thermogravimetric analysis (TGA) and XRD scan were also introduced to observe the hydration products of this model system. Slices cut from the specimens were immersed into isopropanol bath for one week to stop hydration (refreshed every day). Then, they were crushed and

ground to below 63 μm for measurement immediately. TGA was performed with a Netzsch STA 449 F3 Jupiter under argon atmosphere. Approximately 40 mg of the material was heated from 40 to 900 °C with a heating rate of 10 °C/min in an Al_2O_3 crucible and an identical crucible as reference. Besides, the bound water content (BW) was also obtained from thermogravimetric measurement according to: $BW = \left(\frac{W_{50}-W_{550}-W_{H_2OCH}}{W_{550}}\right)$ with W_{50} = sample weight at 50 °C, W_{550} = sample weight at 550 °C and W_{H_2OCH} = mass loss from the decomposition of portlandite by tangent method [41,42]. For XRD measurements, identical procedure was used as mentioned in Section 2.2.

2.3.2. Dissolution test

To gain a more instrumental insight between reactivity and chemical composition, batch dissolution test was carried out. Slag powders with the particle size distribution shown in Fig. 1 were also employed for dissolution test. All slag samples were isolated and reacted in a closed dilute system, and high liquid to solid ratio (1000) allows the dissolution mechanism to be analyzed as much as possible. The concentration of ion release measured provides evidence of the dissolution kinetics of slag under alkaline condition, indicating the reactivity to a certain extent. Although the setup cannot guarantee pure dissolution, it still offers a good approximation to the slag dissolution characteristics in a realistic blended cement system.

Concentrations of the four main ions (Ca^{2+}, Si^{4+}, Al^{3+}, and Mg^{2+}) were measured in NaOH solution with a pH of 13.2 (5.6 g NaOH particle was dissolved in 1000 g deionized water, and the concentration of NaOH was 0.14 M.), corresponding to that of pore solution in a hydrated blended cement paste [37–39]. The experiment was carried out in 1000 mL PE bottle at 20 ± 2 °C. To avoid abrasion, the solution was not stirred while these bottles were put on the rotary table with a small rotor in each of them at a low speed. Solution was sampled at 1, 2, 4, 6, 8, 24, 48 and 72 h (3 days) during test. About 10 mL solution was taken each time, filtered (2.5 μm filter paper) and stored at 4 °C. After each sampling, the same amount of NaOH solution (0.14 M) was added to keep the volume in the bottle constant (1000 mL). The pH of solution was measured with a pH meter 827 Metrohm during the dssolution, and after 7 days, it decreased only a little to around 13.0. The concentrations of Ca, Si, Al and Mg were measured by ICP–OES (Optima 5300 DV) with matrix-matched standard. Concentration below 0.1 mg/L cannot be detected by the equipment. In the preliminary test, replicates were prepared and subjected to the analysis. The variation was within ±3% for the measurement of Ca, Si, Al and Mg concentrations.

After 7 days, dissolution test was stopped, solution was filtered and undissolved particle residue was collected, rinsed with isopropanol, and dried at 40 °C oven for ~10 min. These residues were collected and subsequently ground for TGA measurement.

3. Results

3.1. The characterization of slag

As presented in Fig. 2, it was found that the nine synthetic slags and one commercial slag were almost entirely amorphous with no observed crystal peak which indicated the lack of long-range structural order. For M series, the position of amorphous hump shifted a little bit toward higher diffraction angle with increasing MgO content while it moved to lower angle with decreasing CaO + MgO content (increasing Al_2O_3 content) in A series conversely. Similarly, the position shifted left a small quantity with decreasing CaO/SiO_2 ratio. In fact, the change of the position of amorphous hump was minor, and it fluctuated at about 30° (2θ).

Fig. 3 shows the morphology of commercial slag S and synthetic slag A18 as observed by SEM, all of which were predominantly irregular with clear fracture edges and angles, indicating the existing of glassy phase in the structure of slag.

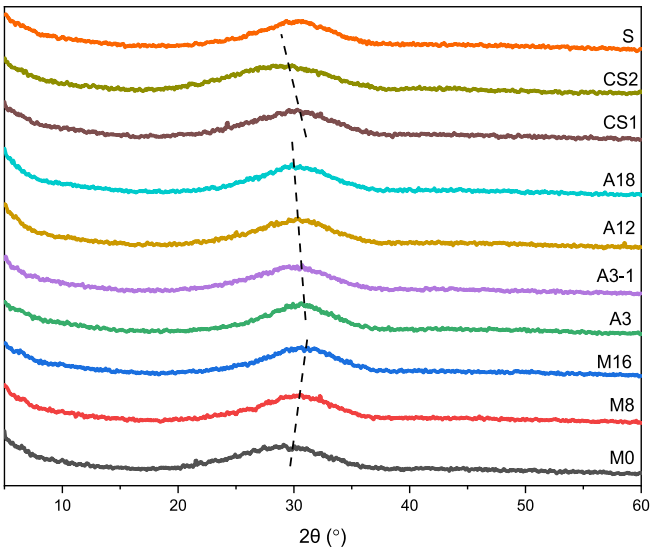

Fig. 2. XRD scans of nine synthetic slags and one commercial slag. The small Bragg peaks in slag M8 and CS1 could be attributed to the formation of akermanite and gehlenite, respectively.

Fig. 4 shows the FTIR spectroscopy results of slag samples within the wave number region between 1200 and 600 cm^{-1}. This region represents the symmetric stretching vibration band of the $[SiO_4]^{4-}$ tetrahedra between 1200 and 760 cm^{-1} and the asymmetric stretching vibration band of the $[AlO_4]^{5-}$ tetrahedra between 760 and 610 cm^{-1}. Moreover, the $[SiO_4]^{4-}$ tetrahedral vibration band could be divided into four characteristic bands further, in terms of $[Si_4O_{10}]^{4-}$ (sheet, 1100–1050 cm^{-1}), $[Si_3O_{10}]^{8-}$ (chain, 980–950 cm^{-1}), $[Si_2O_7]^{6-}$ (dimer, 920–900 cm^{-1}) and $[SiO_4]^{4-}$ (monomer, 880–850 cm^{-1}) respectively [43-46].

From the figure, no clear differences were found between slag samples with different compositions. The broaden absorption band from 800 to 1000 cm^{-1} indicated the existence of different $[SiO_4]^{4-}$ tetrahedral vibration bands. Additionally, it should be noted that the relative intensity of AlO_4 tetrahedra at about 690 cm^{-1} decreased with MgO addition in M series. Probably it was related to the reduction of relative abundance of AlO_4 tetrahedral incorporated into the silicate network. On the contrary, it was foreseeable that the relative intensity of AlO_4 tetrahedra increased with Al_2O_3 addition in A series.

3.2. Reactivity of the slag samples

3.2.1. Hydraulicity test

The hydraulicity/R3 test involves isothermal calorimetry for determining the heat flow and cumulative heat evolution of the model system, and thermogravimetric measurement for determining the amount of chemically bound water in hydrated phases.

3.2.1.1. Calorimetry. The recorded heat flow and cumulative heat release of the model paste after 7 days is presented in Fig. 5 (a) and (b), respectively. The reference sample paste with quartz was also measured under the identical condition. The initial peak, which occurred immediately after mixing with water, was associated with wetting and dissolution of the components. A main peak, indicating the reaction between slag and $Ca(OH)_2$, arose at about 12 h after mixing in all paste samples except the reference. In M series, the heat flow rose significantly with the increasing MgO content, in which the reaction between slag M16 and $Ca(OH)_2$ seemed to be the fastest among all. It resulted in a 52.8% higher total heat release at 7 days in comparison to M0 blend. Similarly, the heat flow went up considerably from A3 to A18 in A series. Among all these slags, A3 and A3-1 which had the least Al_2O_3 content showed the lowest chemical reactivity. In CS series, the difference

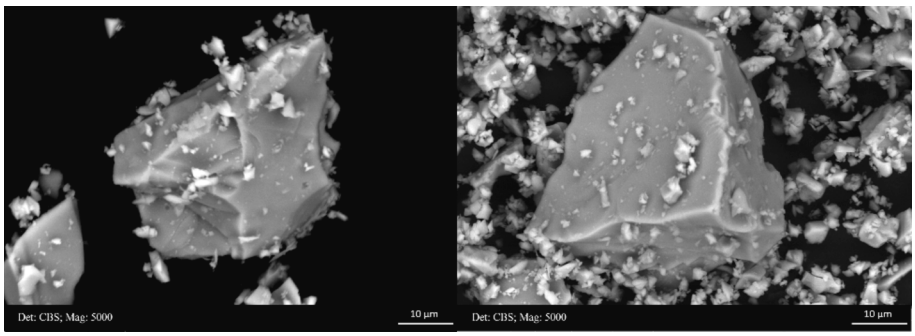

Fig. 3. SEM micrographs of commercial slag S (left) and synthetic slag A18 (right).

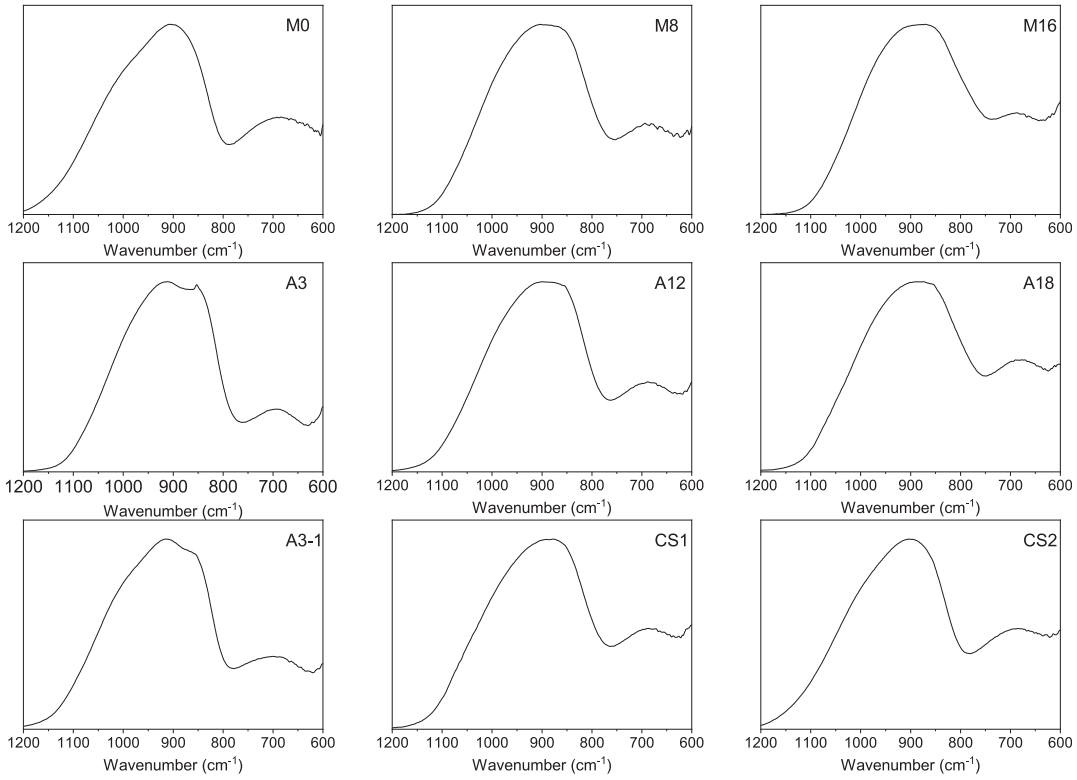

Fig. 4. FTIR spectroscopy results of slag samples in absorbance mode (Normalized, %).

between heat flow and total heat release was very small although the CaO/SiO_2 ratio decreased from 0.85 for CS1 to 0.65 for CS2 (As for CaO + MgO/SiO_2 ratio, it decreased from 1.14 to 0.88 correspondingly.).

Although the chemical composition of commercial slag S was similar to that of M8, and the heat of hydration characteristics were identical during the first 24 h, an additional peak was observed in the model paste with the commerical slag S after the main peak. This peak (labelled A) was analogous to the hump seen in commercial cement system due to the transformation of ettringite into AFm phases [24], which was actually because of the incorporation of sulfur species in commercial slag S (see Section 3.3). The total heat released by the model paste S overtook M8 after one day and reached the highest total heat release eventually.

3.2.1.2. Bound water content. The chemically bound water content against cumulative heat release is plotted in Fig. 6. Considering the relative uncertainty of the whole process, bound water due to the formation of hydrates is clearly visible after 7 days.

Generally, the trend of chemically bound water content among these slags is positively associated with that of 7 days heat release from the calorimetric measurements. Results showed that higher MgO and Al_2O_3 contents led to higher bound water content, and the highest bound water content was detected for the model pastes with synthetic slags M16 and A18, and commercial slag S. Conversely, A3 and A3-1 containing model pastes showed the least amount of chemically bound water. It should be noted that the results represent only a small range of binder mass (~0.05 to ~0.08), which reduces the the reliability of using chemically bound water as an index to distinguish the reactivities of slags.

Further analysis of the results shows that these nine synthetic slags could be roughly classified into two clusters: Cluster I contains slag A3 and A3-1, which shows the least heat release (≤250 J/g) and bound water content (≤0.05); For other slags in cluster II, the bound water contents are similar in these mixtures, in the range of 0.07–0.08.

3.2.1.3. Hydration products. For a clear view, TG and DTG results from five model pastes are shown in Fig. 7. The main hydrates formed in all these blends were similar. The mass loss at 400–500 °C and 700–800 °C were attributed to the dehydration of portlandite and decarbonation of limestone, respectively. Ettringite was observed, and the formation of

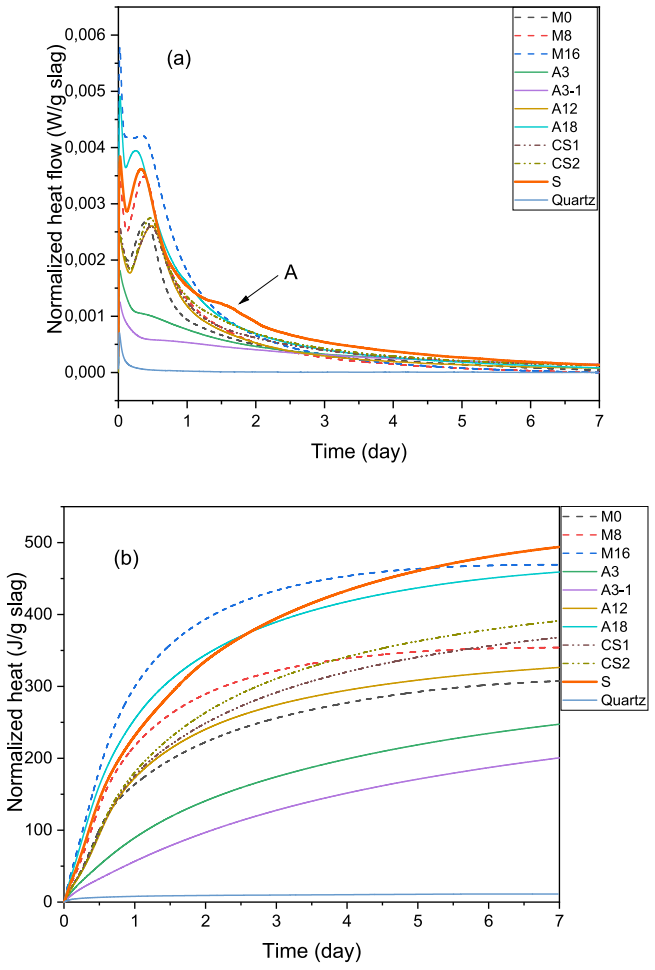

Fig. 5. (a) Heat flow and (b) total heat released as a function of time in calorimetric measurement for the model paste.

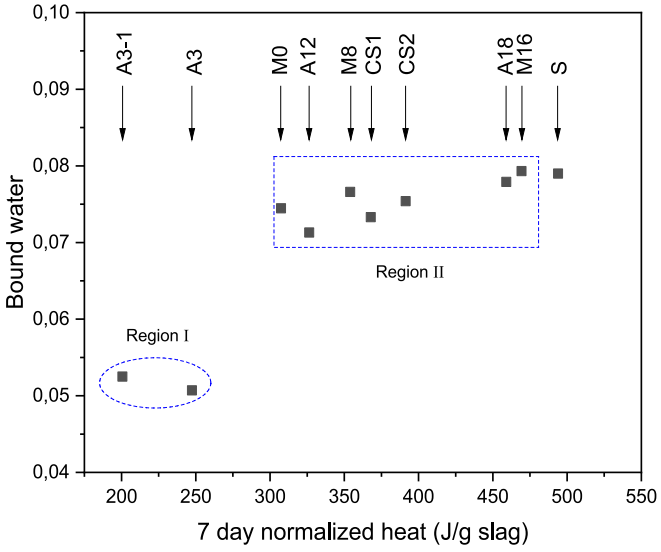

Fig. 6. Bound water content against cumulative heat release.

monocarbonate (Mc) or hemicarbonate (Hc) with the presence of limestone prevented the precipitation of monosulfate (Ms) and stabilized ettringite indirectly [47–49]. Hydrotalcite-like phase (Ht) could also be detected with the provision of MgO and Al_2O_3 from slag. In the M16 mixture, very little precipitation of Mc or Hc was observed whereas a distinct amount of Ht was indicated. This may imply that Al^{3+} ion was more preferable to be incorporated into Ht compared with Mc or Hc. It means that more Ht will be seen in the mixture at the expense of AFm phase with the increasing amount of MgO in slag. Moreover, the authors in [27,50] investigated the potential effect of MgO of slag in alkali activated system, and they also found that the amount of Al incorporation into C–S–H gel phase decreased with increasing MgO content in slag indicated by the low Al/Si atomic ratio. As for the model paste A18, ettringite became unstable and more Mc was detected. When the amount of MgO in slag was fixed as in series A, a distinct dependence on the alumina content of slag and the amount of AFm phase was noticed. Also, the literature showed that the higher the alumina in slag, the more Mc formation was observed [27,50]. For samples A3 and A3-1 (Fig. 7 (c)), peaks seen in other pastes at ~100 and ~200 °C merged into the peak at ~150 °C, and the broaden peak at ~350 °C remained.

Similarly, typical XRD results from five model pastes are presented in Fig. 8. No trace of Ms was detected, and ettringite was observed in all investigated samples except for the pastes of A3 and A18, peaks of which at 2-theta ~9.1 and ~15.8° were undistinguishable. It was also confirmed by TGA result (Fig. 7) that ettringite became unstable, and much more Mc was formed in A18 paste. Despite the reported low crystallinity of carbonate-containing AFm phases such as Mc and Hc, XRD generally allows a distinction between them. Mc was detected without Hc, independently of the chemical composition of slag. It was also found that Hc was the main carbonate bearing phase during the first few days while Mc precipitated at a later stage with the presence of limestone in [24,47,49]. For M16 paste, the peak indicating Ht seemed to dominate over Mc, which was consistent with the TG and DTG results shown in Fig. 7 (b), meaning that more Ht will be observed at the expense of AFm phase with the increasing amount of MgO present in slag. As for A3 paste, lack of peaks indicated a poor crystallinity. Together with the DTG results in Fig. 7 (c), the low Al_2O_3 content in slag A3 and A3-1 will be incorporated into C–S–H gel phase and Ht, rather than taking part in the formation of ettringite or carbonate-bearing AFm phase.

3.2.2. Dissolution test

In slag cement where slag is exposed to highly alkaline environment, OH^- ion attacks the surface of slag, leading to the release of calcium, silicon and aluminum species into pore solution. Once supersaturation has been reached, hydrates such as calcium-silicate (alumino) hydrates (C–S(A)–H), ettringite, AFm phases and a hydrotalcite-like phase start to nucleate and grow [4–6]. Thus, there is a consensus that the hydration process of slag could be regarded as a series of coupled reactions involving the dissolution of slag and precipitation of hydrates, and the dissolution process is strongly associated with its chemical composition.

3.2.2.1. Elemental concentrations. Elemental concentrations (Ca, Si and Al) of five representative slags in the solution is shown in Fig. 9. It was found that an initially nonlinear concentration increase was followed by a linear development for Ca, Si and Al concentrations with time. The observed deceleration of dissolution rate after 1 day was likely to be caused by ion accumulation in the solution, which lowered undersaturation [38], i.e. the driving force for dissolution (Section 3.2.2.2). The concentration of Mg^{2+} ion in the solution was very low, even under the detection limit in some sampling points.

The concentrations of Si^{4+} and Al^{3+} at 3 days against cumulative heat release is shown in Fig. 10. The Si^{4+} concentration in the diluted system showed a significant correlation with 7 days heat release from calorimetric measurement (Fig. 10 (a)). Generally, higher MgO and Al_2O_3 contents led to higher Si^{4+} concentration in the solution. Similarly, these nine synthetic slags could be divided into three regions based on Si^{4+} concentration and cumulative heat release: Region I contains slag A3 and A3-1, which shows the least amount of heat release (≤300 J/

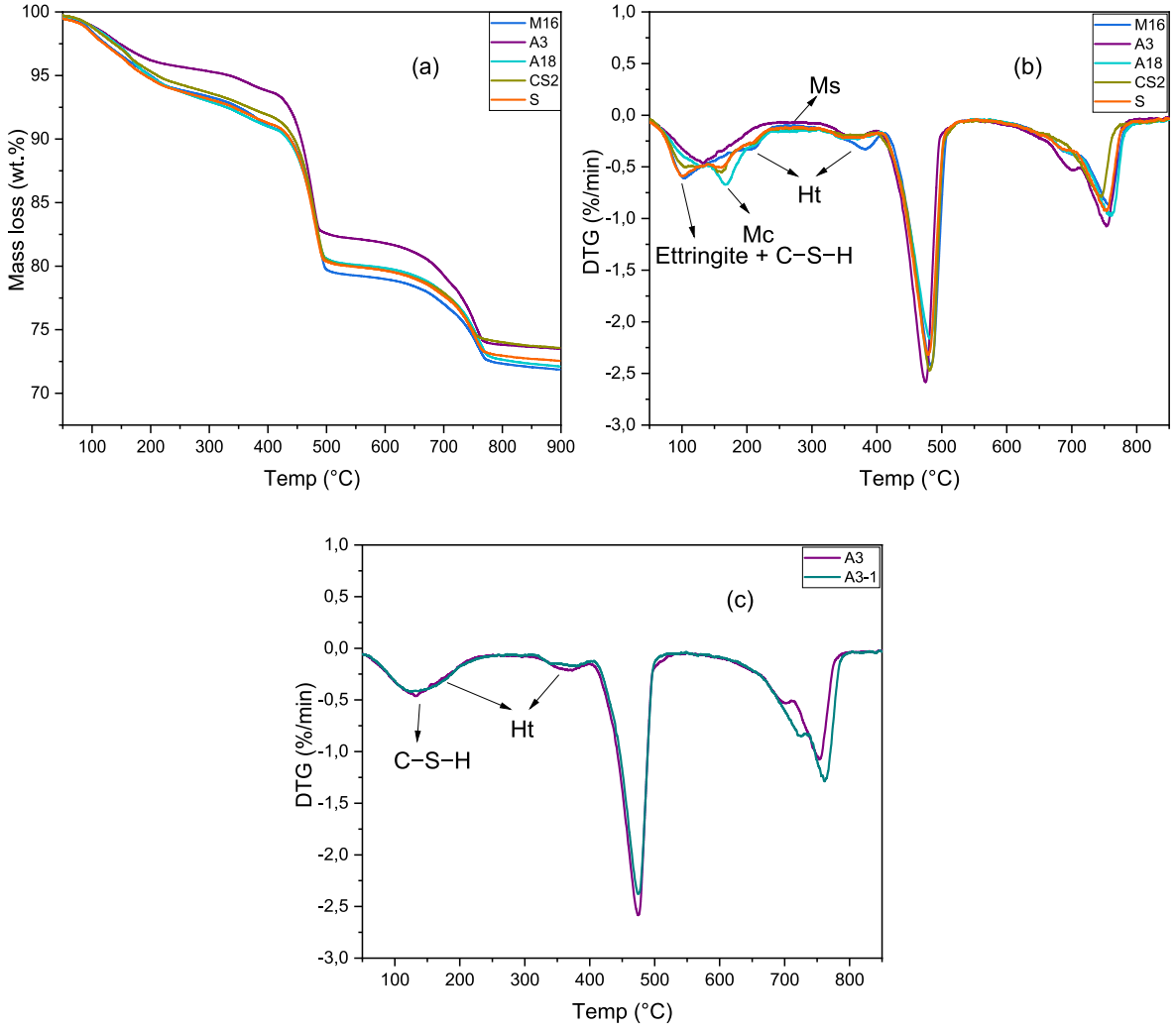

Fig. 7. Typical results of (a) TG and (b and c) DTG analyses of model pastes after 7 days curing at 40 °C. Ht: hydrotalcite-like phase; Mc: monocarbonate; Ms: monosulfate.

g) and Si^{4+} concentration normalized to its molar fraction (≤30 mg/L); Region III represents slag M16 and A18, corresponding to the highest heat release (≥450 J/g) and Si^{4+} concentration (≥45 mg/L); For other slags, they are located in Region II with medium heat release (300–400 J/g) and Si^{4+} concentration (30–45 mg/L). However, the correlation between Al^{3+} concentration and 7 days heat release was not as good as that of Si^{4+} (Fig. 10 (b)). The concentration of Al^{3+} showed a decreasing trend with increasing MgO mass percentage of raw slag with the order: M0 < A12 < CS1 < CS2 < M16 as circled in Fig. 10 (b). Among all, M16 presented an Al^{3+} concentration of ~35 mg/L, only over that of slag A3 and A3-1 although it released the most heat. It was also noted that in contrast to high heat release and bound water content determined from hydraulicity test, commercial slag S only presented a medium Si^{4+} concentration at 3 days.

3.2.2.2. Effective saturation indices. Saturation index (SI) is an indicator to assess which solid phase can form or will dissolve from a thermodynamic point of view. It is given by equation (Eq. (1)), where ion activity product *IAP* is activities derived from the measured concentrations, and K_{so} corresponds to the solubility product of the regarding solid phase. Effective saturation indices (ESI) is determined by dividing the saturation indices by the number of ions participating in the reaction (Eq. (2)) [51,52]. A positive value implies oversaturation when the respective solid phase can form or precipitate while a negative effective saturation index suggests undersaturation with regard to this solid phase, meaning that it cannot form or will dissolve. For the K_{so} values of phases involved in the study, please refer to [53].

$$SI = log\left(\frac{IAP}{K_{so}}\right) \tag{1}$$

$$ESI = \frac{1}{N} log\left(\frac{IAP}{K_{so}}\right) \tag{2}$$

Fig. 11 (a) presents the ESI of slag M8 with respect to hydrotalcite-like phase, brucite and C–S(A)–H gel phase as a function of dissolution time, as an example. It showed clearly that hydrotalcite-like phase and brucite were saturated from the first hour after dissolution. C–S(A)–H gel phase was below saturation at that time, and it was saturated at around 8 h. These precipitations were also confirmed by the DTG results shown in Fig. 11 (b). The mass loss at ~150 and 350 °C were attributed to the dehydration of C–S(A)–H gel phase and hydrotalcite-like phase, respectively. Small shoulders after 500 °C was associated with the decomposition of low crystallinity $Mg(OH)_2$ and its carbonation form $MgCO_3$ [54]. This suggested the fact that aluminum was consumed during the formation of hydrotalcite-like phase. The higher the MgO content of slag, the more aluminum was fixed into hydrotalcite-like phase, which led to a lower amount of Al^{3+} ion available in the solution as confirmed by Fig. 10 (b).

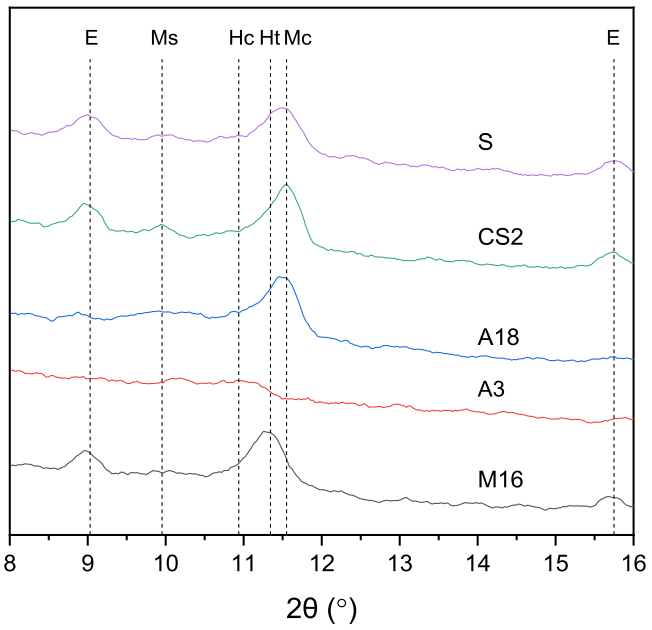

Fig. 8. XRD diffractograms of the selected model pastes after 7 days curing at 40 °C. E – ettringite; Ht: hydrotalcite-like phase; Hc: hemicarbonate; Mc: monocarbonate; Ms: monosulfate.

3.2.2.3. Dissolution rate. The dissolution rate (r_+) using Si^{4+} concentration as indicator was calculated based on the initial increase of Si^{4+} concentration (before 6 h) as the following equation shows [37]:

$$r_+ = \frac{d(Si)}{\Delta t}\frac{v_{Si}V_{solution}}{mS}$$

where v_{Si} represents the molar fraction of Si in raw slag, m designates the mass of slag sample (1.0 g), S corresponds to the initial specific surface area of slag measured by BET method, and $V_{solution}$ is the solution volume (1.0 L). Table 3 summarizes the dissolution rate calculated for all the slag samples.

Basically, the dissolution rates (in Table 3) showed similar trend with regard to the Si^{4+} concentration at 3 days, namely higher MgO (slag M16) and Al_2O_3 (slag A18) contents lead to a higher dissolution rate. On the other hand, it should be noted that the solution started to be saturated from the beginning regarding Mg-bearing phases (brucite and hydrotalcite-like phase) as confirmed by effective saturation indices. Thus, more research is needed to figure out whether these precipitations have any impact on the release of Si from slag. Moreover, the relatively high dissolution rate of slag M0 could be explained by its small specific surface area (Table 1).

3.3. The effect of sulfur species in commercial slag

Sulfur content in slag is generally determined in the form of SO_3 by XRF. The presence of several sulfur anions, such as S^{2-}, $S_2O_3^{2-}$ and SO_4^{2-}, has been reported in leachates of hydrated cement containing slag [55-57]. Oxidation to the most stable product, i.e. SO_4^{2-} can take place by molecular oxygen at pH greater than 8.5 considering the alkaline and mildly reductive environment occurring in the pore solution of slag cement [58]. In this paper for the production of synthetical slag, the remelting process of commercial slag was under oxidizing condition (non-inert atmosphere), whereas the real commercial slag provided by Ecocem Benelux B.V. was produced under reducing condition. The oxidizing condition might modify the oxidation state of sulphur species in slag, likely shifting it towards more oxidized species or straight-out volatilizing it. It explains the low SO_3 content detected in synthetical slag.

As presented earlier in Fig. 5 (a), an additional peak or hump was observed in the model paste of commercial slag S after the main peak. To investigate this phenomenon, we introduced another commercial slag, S1 (also provided by Ecocem Benelux B.V.). Its chemical composition was determined in wt.% by XRF as; CaO: 37.97%, SiO_2: 35.6%, Al_2O_3: 13.12%, MgO: 7.24%, FeO/Fe_2O_3: 0.37%, MnO/Mn_2O_3: 0.35%, Na_2O: 0.31%, SO_3: 0.99%, Residual: 4.05%. The loss-on-ignition (LOI) determined by TGA under air environment at 950 ± 50 °C for commercial slag S and S1 was −0.87% and −1.27%, respectively. This value was −0.02% for synthetic slag M8. The negative LOI is related to the oxidation of sulfur rich species in slag when exposed to air. Slag M8, S and S1 had a similar chemical composition except the sulfur content. It is worthwhile to mention that the exact thermal history of commercial slag was unknown. The authors received the coarse-granulated slag S and S1 from Ecocem Benelux B.V. and milled them to a similar PSD with other synthetic slags subsequently.

Fig. 12 illustrates the heat flow and cumulative heat release of model pastes of M8, S and S1 after 7 days at 40 °C. As labelled (A), the additional peak was only observed right after the main peak for commercial slag S and S1 although the time of occurrence was slightly different. It was also apparent that the curves of cumulative heat release overlapped with each other up to about 24 h and derivated from then on as depicted in Fig. 12 (b). About 150 J/g slag more heat was released by commercial slag S and S1 compared with synthetic slag M8 after 7 days due to the hump. Moreover, when checked in TGA measurement as displayed in Fig. 13, the peak at about 100 °C was more distinct in the model pastes S and S1, and the amounts of portlandite remained in S and S1 pastes decrease compared with that of M8. Therefore, it is plausible to assume that the additional peak A originates from the precipitation of ettringite following the equation:

$6Ca^{2+} + 2AlO^{2-} + 3SO_4^{2-} + \boldsymbol{4OH^-} + 30H_2O \rightarrow Ca_6Al_2(SO_4)_3(OH)_{12}{\cdot}26H_2O$ $\Delta_f H^0 = -17535 kJ/mol$ [59].

Considering the enthalpy of formation $\Delta_f H^0$ of ettringite, it was calculated that $\sim 2.5 \times 10^{-3}$ g SO_4^{2-}/g slag participated in the reaction. This is reasonable as the oxidation of reduced sulfur species occurs when water is consumed and sufficient air enters the paste sample.

On the other hand, it should be noted that the above observation was based on a TGA peak that could be assigned to both C–S–H gel phase and ettringite. For a clearer attribution, evidence showing that the amount of ettringite (significantly) increases is preferred. Moreover, questions, e.g. why the sulphur species in slag is released only at a specific point (A) after the main hydration peak, and the model paste already contains sulfate contributed by the potassium solution still remain unsolved. Therefore, more properties should be explored in the following studies such as the effect of minor elements, quenching rate, etc.

4. Discussion

In order to assess the reactivity of blast furnace slag, efforts have been made to observe a relationship which could be used to predict slag reactivity from its chemical composition [16,60]. Hydraulic moduli, or Basicity, categorized into different types were reviewed in [18]. However, none of them gives a satisfactory result for a general estimation of reactivity of various slag used in cement [19,60]. Besides, the reactivity of slag could also be attributed to the network structure of glass. The more disordered and depolymerized a structure is, the more easily it can be broken up, and show higher reactivity. The degree of depolymerization of a network structure can be represented by NBO/T, the number of non-bridging oxygen per tetrahedral network-forming element [61,62]. In all slags investigated in this paper, considering $Al_2O_3 < 0.5$ SiO_2 in molar ratio, Al should be regarded as network former existing only in-between SiO_4 tetrahedra in the form of Si–O–Al–O–Si (Loewenstein's rule of aluminum avoidance [8]), and the charge difference between AlO_4^{5-} and SiO_4^{4-} tetrahedra was balanced by Ca^{2+} and K^+, in principle [9,10,63]. However, it was noted that more heat was released from calorimetry measurement, more bound water was fixed in the

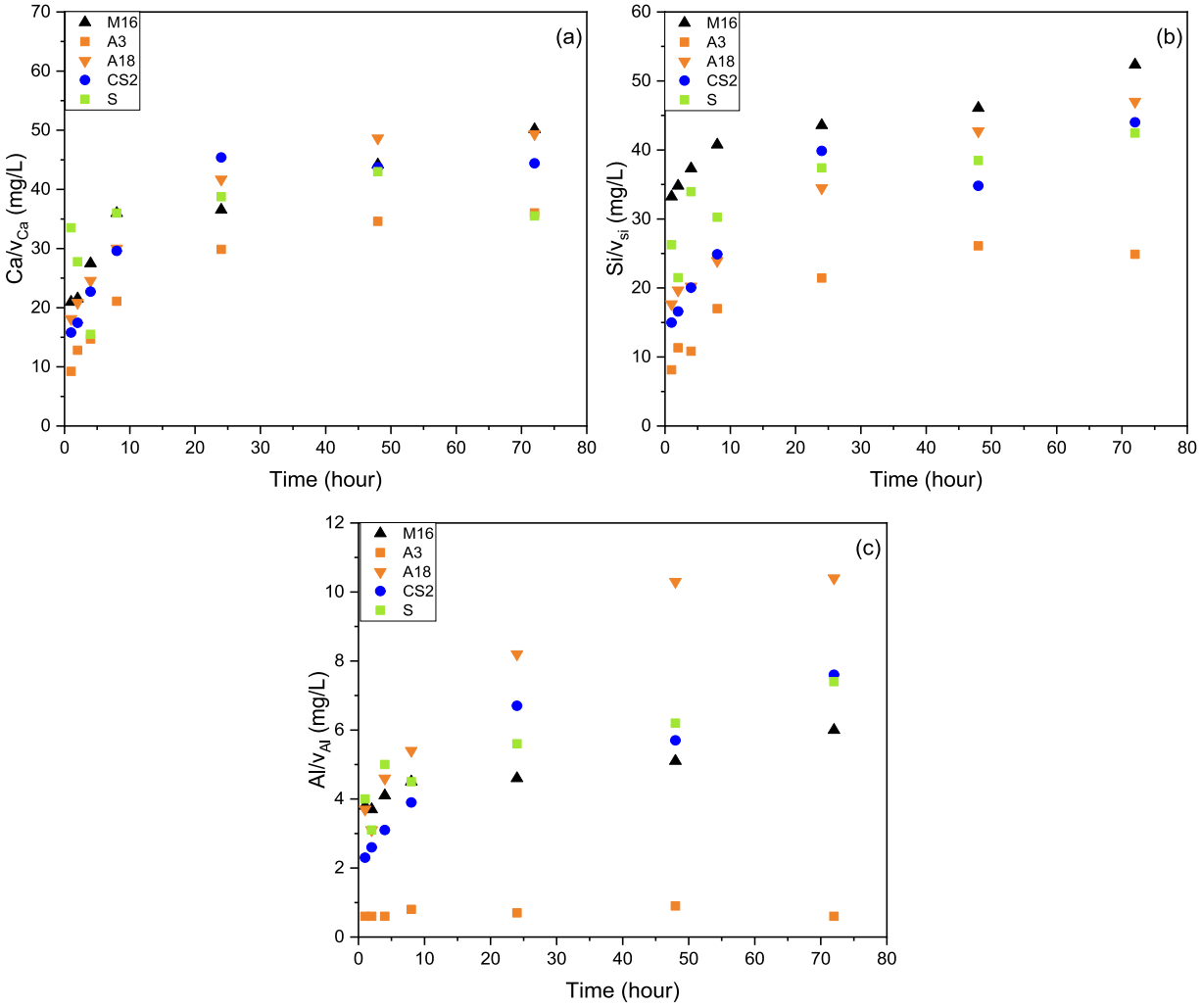

Fig. 9. (a) Ca^{2+} (b) Si^{4+} and (c) Al^{3+} ion concentrations in the solution normalized to their molar fractions in raw slag, respectively plotted in function of time up to 3 days.

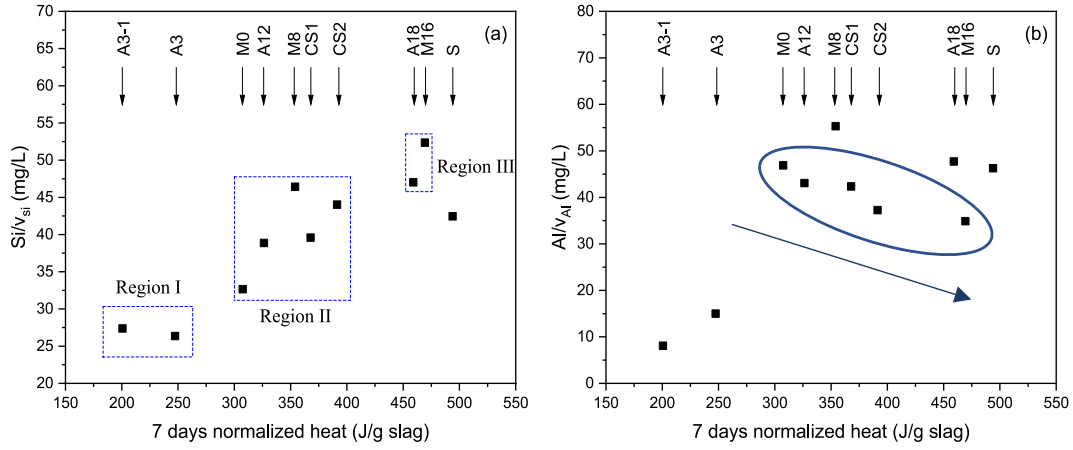

Fig. 10. (a) Si^{4+} and (b) Al^{3+} concentrations in the solution normalized to their molar fraction in raw slag, respectively against cumulative heat release.

hydrates, and higher concentration of Si was observed in the dissolution test with increasing Al_2O_3 content, in contrast to the values determined by NBO/T (Table 1).

In this study, we attempted to estimate the reactivity of slag through assessing its chemical composition from a new perspective, using a graphical method. The method classifies the reactivity of slag into different regions based on their main oxide compositions. The slags located at each region present ***a similar performance*** based on above tests. Additionally, the graph can explain the interaction among oxides of slag directly. It is based on a coordinate system of (CaO/SiO_2)−(MgO

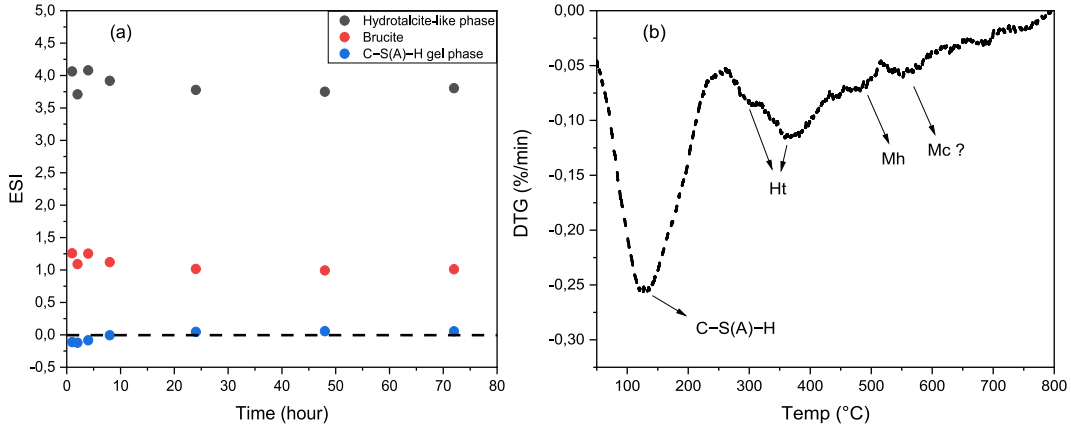

Fig. 11. (a) Effective saturation indices of slag M8 as a function of dissolution time. A saturation index of 0.0 indicates an equilibrium state; (b) DTG result of the undissolved residual after 7 days dissolution test. Mh denotes $Mg(OH)_2$ (brucite) and Mc denotes $MgCO_3$, which may be originated from the carbonation of Mh during sample preparation. Ht: hydrotalcite-like phase.

Table 3
Dissolution rate of slag calculated based on the Si^{4+} concentration from dissolution test.

Slag	M0	M8	M16	A3	A3-1	A12	A18	CS1	CS2	S
Si^{4+} Dissolution rate $\times 10^{-8}$ (mol/m^2/s)	0.63	0.53	0.69	0.39	0.44	0.60	0.69	0.57	0.62	0.76

a. Based on effective saturation indices determined in Section 3.2.2.2, C–S(A)–H gel phase became supersaturated at different time. For comparison, data at 6 h of dissolution was used for calculation. At this stage, the main driving force for dissolution was undersaturation degree and Si-bearing phase was still undersaturated for most slag samples.

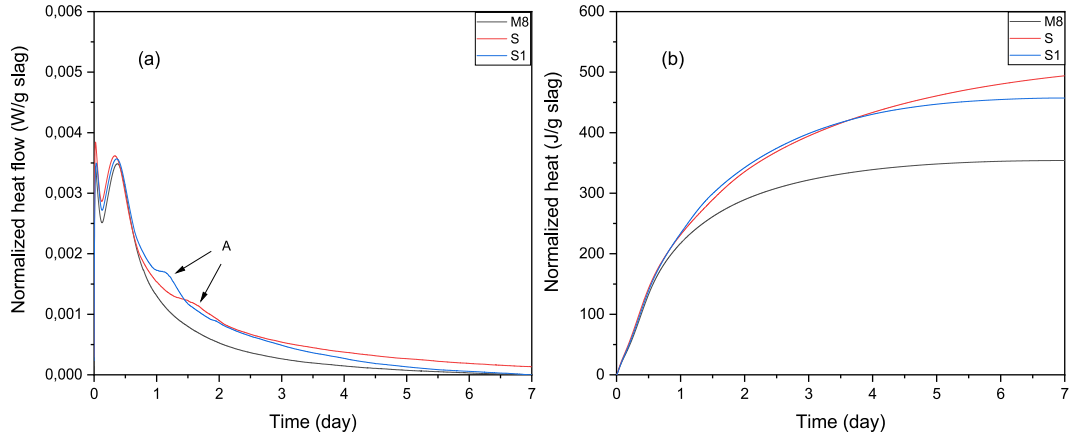

Fig. 12. (a) Heat flow and (b) total heat release as a function of time from calorimetric measurement of model pastes curing for 7 days at 40 °C.

$+ Al_2O_3$) in weight percentage. The accuracy of this method was verified by the results of the current study.

In $(CaO/SiO_2)-(Al_2O_3 + MgO)$ coordinate system of weight percentage as employed in Fig. 14, the effect of Al_2O_3 and MgO was highlighted. The coordinate system could be divided into three regions following: $Al_2O_3 + MgO < 15$ wt% (Region I), $15 < Al_2O_3 + MgO < 25$ wt% (Region II), and $Al_2O_3 + MgO > 25$ wt% (Region III). The position of a slag in each region corresponded to the reactivity determined based on cumulative heat release (Fig. 5), chemically bound water (Fig. 6), Si^{4+} concentration (Fig. 10 (a)), and dissolution rate (Table 3). Region I involves slag with low Al_2O_3 and/or MgO contents showing low reactivity, while Region III represents slag with high Al_2O_3 and/or MgO contents presenting high reactivity. For other slags, they are included in Region II with medium Al_2O_3 and/or MgO contents and medium reactivity.

As for synthetic slag CS1 and CS2, the CaO/SiO_2 ratio of which is<1, are not frequently used in the industry, however, the negative effect of decreasing CaO/SiO_2 ratio on reactivity was compensated by high Al_2O_3 and MgO contents. The graphical method proposed is able to recognize reactive slags accurately while standard moduli can misinterpret their performance. For example, slag CS2 shows a relatively medium reactivity due to its high Al_2O_3 and MgO contents, however hydralicity modulus of EN 15167-1 classifies this slag as unsufficiently reactive through $(CaO + MgO)/SiO_2 = 0.88 < 1.0$.

5. Conclusion

This study proposes new insight on the influence of chemical composition on the slag reactivity. The methodologies proposed in this study appears to have potential for further use in classifying slag reactivity and could lead to formulating improved blast furnace slag compositions for better durability performance. The main conclusions are:

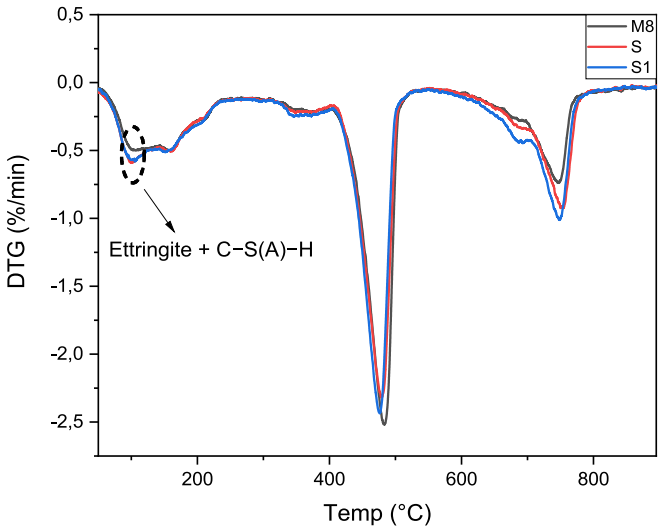

Fig. 13. DTG analysis of model pastes curing for 7 days at 40 °C.

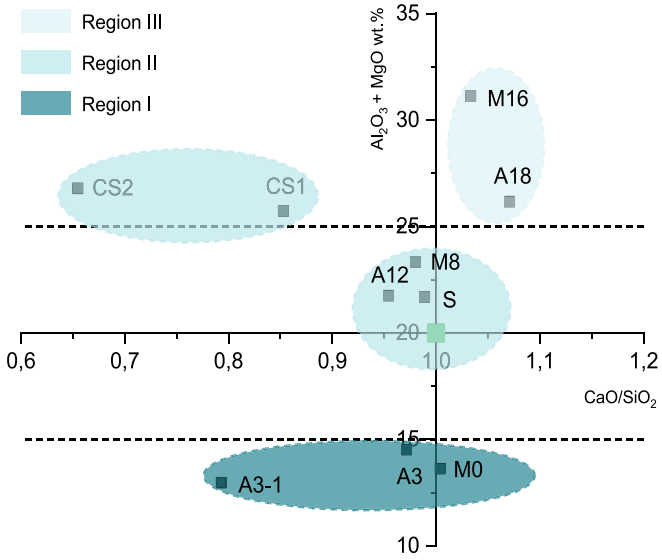

Fig. 14. $(CaO/SiO_2)-(Al_2O_3 + MgO)$ coordinate system in weight percentage. For the weight composition of these synthesized slags, please see data in Table 1. The green square in the coordinate system represents slag containing CaO: 40%, SiO_2: 40%, Al_2O_3: 10%, MgO: 10% by mass, and this chemical composition of slag is most commonly seen in the industry.

- The reactivity determined from calorimetric measurement and bound water content quantification of the model pastes containing synthetic slag, portlandite, limestone and alkaline solution follows similar tendency.
- According to results of the dissolution test with high liquid to solid ratio system, Si^{4+} concentration and its dissolution rate supports the findings from the calorimetric measurements. Higher MgO and Al_2O_3 contents of slag lead to a higher dissolution rate.
- MgO effectively favors the formation of hydrotalcite-like phase over AFm phases. As for Al_2O_3, it prefers to be shared by the formations of hydrotalcite-like phase and C–S(A)–H at a low mass percentage, while it promotes transformation of ettringite into AFm phase (monocarbonate here) as the alumina content of slag increases.
- The sulfur species in slag causes the additional peak in the model paste of commercial slag S and S1 in calorimetric measurements. It originates from the precipitation of ettringite. Therefore, when calorimetric measurement is used to assess the reactivity of slag, the effect of sulfur species must be taken into consideration as even a small quantity of it could lead to a large difference of cumulative heat release.
- A graphical methods based on $(CaO/SiO_2)-(Al_2O_3 + MgO)$ coordinate system in weight percentage, was proposed to be used to estimate the reactivity of slag. It was also found that the adverse effect of decreasing CaO/SiO_2 ratio on reactivity could be compensated by higher Al_2O_3 and/or MgO contents which can be recognized with the proposed graphical method.

CRediT authorship contribution statement

Yu Zhang: Investigation, Methodology, Writing – original draft, Writing – review & editing. **Shizhe Zhang:** Methodology, Writing – review & editing. **Yu Chen:** Writing – review & editing. **Oğuzhan Çopuroğlu:** Supervision, Funding acquisition, Writing – review & editing.

Declaration of Competing Interest

The authors declare that they have no known competing financial interests or personal relationships that could have appeared to influence the work reported in this paper.

Acknowledgements

China Scholarship Council (the Grant Number 201808320456 and 201807720005) and BAM Infraconsult B.V. are gratefully acknowledged for their financial support. Authors thank John van den Berg (Microlab, TU Delft) for their technical support. Jeanette van den Bos (BAM Infraconsult B.V.) and René Albers (Ecocem Benelux B.V.) are gratefully acknowledged for the technical discussions and providing commercial slags.

References

[1] E. Gartner, Industrially interesting approaches to “low-CO2” cements, Cem. Concr. Res. 34 (9) (2004) 1489–1498.
[2] M.C.G. Juenger, F. Winnefeld, J.L. Provis, J.H. Ideker, Advances in alternative cementitious binders, Cem. Concr. Res. 41 (12) (2011) 1232–1243.
[3] Y. Li, Y.u. Liu, X. Gong, Z. Nie, S. Cui, Z. Wang, W. Chen, Environmental impact analysis of blast furnace slag applied to ordinary Portland cement production, J. Cleaner Prod. 120 (2016) 221–230.
[4] W. Chen, H.J.H. Brouwers, The hydration of slag, part 2: reaction models for blended cement, J. Mater. Sci. 42 (2) (2006) 444–464.
[5] B. Kolani, L. Buffo-Lacarrière, A. Sellier, G. Escadeillas, L. Boutillon, L. Linger, Hydration of slag-blended cements, Cem. Concr. Compos. 34 (9) (2012) 1009–1018.
[6] E. Özbay, M. Erdemir, H.İ. Durmuş, Utilization and efficiency of ground granulated blast furnace slag on concrete properties – A review, Constr. Build. Mater. 105 (2016) 423–434.
[7] K. Shimoda, Y. Tobu, K. Kanehashi, T. Nemoto, K. Saito, Total understanding of the local structures of an amorphous slag: perspective from multi-nuclear (29Si, 27Al, 17O, 25Mg, and 43Ca) solid-state NMR, J. Non-Cryst. Solids 354 (10-11) (2008) 1036–1043.
[8] W. Loewenstein, The distribution of aluminum in the tetrahedra of silicates and aluminates, Am. Mineral. 39 (1–2) (1954) 92–96.
[9] C.I. Merzbacher, B.L. Sherriff, J.S. Hartman, W.B. White, A high-resolution 29Si and 27Al NMR study of alkaline earth aluminosilicate glasses, J. Non-Cryst. Solids 124 (2-3) (1990) 194–206.
[10] D.R. Neuville, L. Cormier, D. Massiot, Al coordination and speciation in calcium aluminosilicate glasses: Effects of composition determined by 27Al MQ-MAS NMR and Raman spectroscopy, Chem. Geol. 229 (1-3) (2006) 173–185.
[11] K.C. Mills, L. Yuan, Z. Li, G.H. Zhang, K.C. Chou, A review of the factors affecting the thermophysical properties of silicate slags, High Temp. Mater. Processes 31 (4-5) (2012) 301–321.
[12] I. Sohn, D.J. Min, A review of the relationship between viscosity and the structure of calcium-silicate-based slags in ironmaking, Steel Res. Int. 83 (7) (2012) 611–630.
[13] K.C. Mills, The influence of structure on the physico-chemical properties of slags, ISIJ Int. 33 (1) (1993) 148–155.
[14] W. Xuan, J. Zhang, D. Xia, The influence of MgO on the crystallization characteristics of synthetic coal slags, Fuel 222 (2018) 523–528.

[15] S. Zhang, X.i. Zhang, W. Liu, X. Lv, C. Bai, L. Wang, Relationship between structure and viscosity of CaO–SiO2–Al2O3–MgO–TiO2 slag, J. Non-Cryst. Solids 402 (2014) 214–222.
[16] J.I. Escalante, L.Y. Gómez, K.K. Johal, G. Mendoza, H. Mancha, J. Méndez, Reactivity of blast-furnace slag in Portland cement blends hydrated under different conditions, Cem. Concr. Res. 31 (10) (2001) 1403–1409.
[17] N.e.a. De Belie, Properties of fresh and hardened concrete containing supplementary cementitious materials, vol. 25, Springer, 2018.
[18] ASTM, ASTM C125-Standard Terminology Relating to Concrete and Concrete Aggregates, ASTM International West Conshohocken, 2018.
[19] S. Blotevogel, et al., Ability of the R3 test to evaluate differences in early age reactivity of 16 industrial ground granulated blast furnace slags (GGBS), Cem. Concr. Res. 130 (2020), 105998.
[20] H.F.W. Taylor (Ed.), Cement chemistry, Thomas Telford Publishing, 1997.
[21] P. Barnes, J. Bensted, Structure and Performance of Cements, CRC Press, 2002.
[22] T. Itoh, Rapid discrimination of the character of the water-cooled blast furnace slag used for Portland slag cement, J. Mater. Sci. 39 (2004) 2191–2193.
[23] S.A. Bernal, R. San Nicolas, R.J. Myers, R. Mejía de Gutiérrez, F. Puertas, J.S.J. van Deventer, J.L. Provis, MgO content of slag controls phase evolution and structural changes induced by accelerated carbonation in alkali-activated binders, Cem. Concr. Res. 57 (2014) 33–43.
[24] M. Whittaker, M. Zajac, M. Ben Haha, F. Bullerjahn, L. Black, The role of the alumina content of slag, plus the presence of additional sulfate on the hydration and microstructure of Portland cement-slag blends, Cem. Concr. Res. 66 (2014) 91–101.
[25] E. Pustovgar, R.K. Mishra, M. Palacios, J.-B. d'Espinose de Lacaillerie, T. Matschei, A.S. Andreev, H. Heinz, R. Verel, R.J. Flatt, Influence of aluminates on the hydration kinetics of tricalcium silicate, Cem. Concr. Res. 100 (2017) 245–262.
[26] A. Gruskovnjak, B. Lothenbach, F. Winnefeld, R. Figi, S.-C. Ko, M. Adler, U. Mäder, Hydration mechanisms of super sulphated slag cement, Cem. Concr. Res. 38 (7) (2008) 983–992.
[27] M.B. Haha, B. Lothenbach, G. Le Saout, F. Winnefeld, Influence of slag chemistry on the hydration of alkali-activated blast-furnace slag — Part II: Effect of Al2O3, Cem. Concr. Res. 42 (1) (2012) 74–83.
[28] P.T. Durdziński, R. Snellings, C.F. Dunant, M.B. Haha, K.L. Scrivener, Fly ash as an assemblage of model Ca–Mg–Na-aluminosilicate glasses, Cem. Concr. Res. 78 (2015) 263–272.
[29] A. Schöler, F. Winnefeld, M.B. Haha, B. Lothenbach, The effect of glass composition on the reactivity of synthetic glasses, J. Am. Ceram. Soc. 100 (6) (2017) 2553–2567.
[30] S. Kucharczyk, M. Zajac, C. Stabler, R.M. Thomsen, M. Ben Haha, J. Skibsted, J. Deja, Structure and reactivity of synthetic CaO-Al2O3-SiO2 glasses, Cem. Concr. Res. 120 (2019) 77–91.
[31] S. Kucharczyk, J. Deja, M. Zajac, Effect of slag reactivity influenced by alumina content on hydration of composite cements, J. Adv. Concr. Technol. 14 (9) (2016) 535–547.
[32] S. Nie, et al., Impact of Mg substitution on the structure and pozzolanic reactivity of calcium aluminosilicate (CaO-Al2O3-SiO2) glasses, Cem. Concr. Res. 138 (2020), 106231.
[33] X. Li, R. Snellings, M. Antoni, N.M. Alderete, M. Ben Haha, S. Bishnoi, Ö. Cizer, M. Cyr, K. De Weerdt, Y. Dhandapani, J. Duchesne, J. Haufe, D. Hooton, M. Juenger, S. Kamali-Bernard, S. Kramar, M. Marroccoli, A.M. Joseph, A. Parashar, C. Patapy, J.L. Provis, S. Sabio, M. Santhanam, L. Steger, T. Sui, A. Telesca, A. Vollpracht, F. Vargas, B. Walkley, F. Winnefeld, G. Ye, M. Zajac, S. Zhang, K.L. Scrivener, Reactivity tests for supplementary cementitious materials: RILEM TC 267-TRM phase 1, Mater. Struct. 51 (6) (2018).
[34] R.D. Kalina, S. Al-Shmaisani, R.D. Ferron, M.C.G. Juenger, False Positives in ASTM C618 Specifications for Natural Pozzolans, ACI Mater. J. 116 (1) (2019).
[35] J. Skibsted, R. Snellings, Reactivity of supplementary cementitious materials (SCMs) in cement blends, Cem. Concr. Res. 124 (2019), 105799.
[36] R. Snellings, et al., Rapid, Robust, and Relevant (R3) Reactivity Test for Supplementary Cementitious Materials, ACI Mater. J. 116 (4) (2019).
[37] R. Snellings, C. Jantzen, Solution-Controlled Dissolution of Supplementary Cementitious Material Glasses at pH 13: The Effect of Solution Composition on Glass Dissolution Rates, J. Am. Ceram. Soc. 96 (8) (2013) 2467–2475.
[38] R. Snellings, G. Scherer, Surface Chemistry of Calcium Aluminosilicate Glasses, J. Am. Ceram. Soc. 98 (1) (2015) 303–314.
[39] K.C. Newlands, M. Foss, T. Matchei, J. Skibsted, D.E. Macphee, Early stage dissolution characteristics of aluminosilicate glasses with blast furnace slag- and fly-ash-like compositions, J. Am. Ceram. Soc. 100 (5) (2017) 1941–1955.
[40] K. Mills, et al., Estimating the physical properties of slags, J. Southern Afr. Inst. Min. Metall. 111 (10) (2011) 649–658.
[41] O.R. Ogirigbo, L. Black, Influence of slag composition and temperature on the hydration and microstructure of slag blended cements, Constr. Build. Mater. 126 (2016) 496–507.
[42] A. Bougara, C. Lynsdale, N.B. Milestone, Reactivity and performance of blastfurnace slags of differing origin, Cem. Concr. Compos. 32 (4) (2010) 319–324.
[43] B.O. Mysen, et al., The influence of TiO2 on the structure and derivative properties of silicate melts, Am. Mineral. 65 (11–12) (1980) 1150–1165.
[44] Y. Sun, Z. Zhang, L. Liu, X. Wang, FTIR, Raman and NMR investigation of CaO–SiO2–P2O5 and CaO–SiO2–TiO2–P2O5 glasses, J. Non-Cryst. Solids 420 (2015) 26–33.
[45] G.-H. Kim, I. Sohn, Effect of Al2O3 on the viscosity and structure of calcium silicate-based melts containing Na2O and CaF2, J. Non-Cryst. Solids 358 (12–13) (2012) 1530–1537.
[46] S.-M. Han, J.-G. Park, I.l. Sohn, Surface kinetics of nitrogen dissolution and its correlation to the slag structure in the CaO-SiO2, CaO-Al2O3, and CaO-SiO2-Al2O3 slag system, J. Non-Cryst. Solids 357 (15) (2011) 2868–2875.
[47] A. Schöler, B. Lothenbach, F. Winnefeld, M. Zajac, Hydration of quaternary Portland cement blends containing blast-furnace slag, siliceous fly ash and limestone powder, Cem. Concr. Compos. 55 (2015) 374–382.
[48] S. Adu-Amankwah, M. Zajac, C. Stabler, B. Lothenbach, L. Black, Influence of limestone on the hydration of ternary slag cements, Cem. Concr. Res. 100 (2017) 96–109.
[49] T. Matschei, B. Lothenbach, F.P. Glasser, The role of calcium carbonate in cement hydration, Cem. Concr. Res. 37 (4) (2007) 551–558.
[50] S. Kucharczyk, M. Zajac, J. Deja, The Influence of Limestone and Al2O3 Content in the Slag on the Performance of the Composite Cements, Proc. Eng. 108 (2015) 402–409.
[51] B. Lothenbach, G. Le Saout, E. Gallucci, K. Scrivener, Influence of limestone on the hydration of Portland cements, Cem. Concr. Res. 38 (6) (2008) 848–860.
[52] B. Lothenbach, Thermodynamic equilibrium calculations in cementitious systems, Mater. Struct. 43 (10) (2010) 1413–1433.
[53] T. Matschei, B. Lothenbach, F.P. Glasser, Thermodynamic properties of Portland cement hydrates in the system CaO–Al2O3–SiO2–CaSO4–CaCO3–H2O, Cem. Concr. Res. 37 (10) (2007) 1379–1410.
[54] R.S. Karen Scrivener, Barbara Lothenbach, A Practical Guide to Microstructural Analysis of Cementitious Materials, CRC Press, New York, 2016.
[55] F.P. Glasser, K. Luke, M.J. Angus, Modification of cement pore fluid compositions by pozzolanic additives, Cem. Concr. Res. 18 (2) (1988) 165–178.
[56] A. Gruskovnjak, B. Lothenbach, L. Holzer, R. Figi, F. Winnefeld, Hydration of alkali-activated slag: comparison with ordinary Portland cement, Adv. Cem. Res. 18 (3) (2006) 119–128.
[57] B. Lothenbach, G. Le Saout, M. Ben Haha, R. Figi, E. Wieland, Hydration of a low-alkali CEM III/B–SiO2 cement (LAC), Cem. Concr. Res. 42 (2) (2012) 410–423.
[58] W.E. Kleinjan, A.d. Keizer, A.J.H. Janssen, Kinetics of the chemical oxidation of polysulfide anions in aqueous solution, Water Res. 39 (17) (2005) 4093–4100.
[59] B. Lothenbach, T. Matschei, G. Möschner, F.P. Glasser, Thermodynamic modelling of the effect of temperature on the hydration and porosity of Portland cement, Cem. Concr. Res. 38 (1) (2008) 1–18.
[60] W. Matthes, et al., Ground granulated blast-furnace slag, in: Properties of fresh and hardened concrete containing supplementary cementitious materials, Springer, 2018, pp. 1–53.
[61] D. Dutt, et al., A structural model for low silica content calcium aluminosilicate glasses, Phys. Chem. Glasses 33 (2) (1992) 51–55.
[62] A. Novatski, A. Steimacher, A.N. Medina, A.C. Bento, M.L. Baesso, L.H.C. Andrade, S.M. Lima, Y. Guyot, G. Boulon, Relations among nonbridging oxygen, optical properties, optical basicity, and color center formation in CaO–MgO aluminosilicate glasses, J. Appl. Phys. 104 (9) (2008) 094910.
[63] D.R. Neuville, L. Cormier, V. Montouillout, D. Massiot, Local Al site distribution in aluminosilicate glasses by 27Al MQMAS NMR, J. Non-Cryst. Solids 353 (2) (2007) 180–184.